ADVANCING EARTH AND SPACE SCIENCES

Geophysical Research Letters

RESEARCH LETTER
10.1029/2025GL115186

Key Points:

- The Trans-Heliospheric Survey consists of over 60-years of in-situ solar-wind measurements from over 13 spacecraft
- Trends in solar-wind speed and magnetic field strength with distance from the Sun closely follow the Parker (1958, https://doi.org/10.1086/146579) model

Correspondence to:
C. P. Brown,
carsonb@udel.edu

Citation:
Brown, C. P., Maruca, B. A., Prabakaran, V., Qudsi, R. A., Walsh, B. M., Alterman, B. L., & Isenberg, P. A. (2025). Evaluating the Parker model with the Trans-Heliospheric Survey. *Geophysical Research Letters*, *52*, e2025GL115186. https://doi.org/10.1029/2025GL115186

Received 3 FEB 2025
Accepted 5 JUN 2025

Evaluating the Parker Model With the Trans-Heliospheric Survey

Carson P. Brown[1], Bennett A. Maruca[1,2], Vaishali Prabakaran[3,4], Ramiz A. Qudsi[4], B. M. Walsh[4,5], B. L. Alterman[6], and Philip A. Isenberg[7,8]

[1]Department of Physics and Astronomy, University of Delaware, Newark, DE, USA, [2]Bartol Research Institute, University of Delaware, Newark, DE, USA, [3]Department of Computer Science, Boston University, Boston, MA, USA, [4]Center for Space Physics, Boston University, Boston, MA, USA, [5]Department of Mechanical Engineering, Boston University, Boston, MA, USA, [6]NASA Goddard Space Flight Center, Greenbelt, MD, USA, [7]Space Science Center, University of New Hampshire, Durham, NH, USA, [8]Department of Physics and Astronomy, University of New Hampshire, Durham, NH, USA

Abstract The solar wind's expansion through the heliosphere is often studied by "radial trends"—the average trends in fluid parameters as functions of radial distance from the Sun. This study utilizes the latest version of the Trans-Heliospheric Survey, a compilation of in-situ magnetic field and proton measurements from 13 different spacecraft spanning over 60 years and three orders of magnitude in radial distance to explore global changes throughout the heliosphere. These data are used to evaluate theoretical models, in particular the Parker model of the solar wind's bulk speed and magnetic field. The Parker model matches the speed data well in the inner heliosphere, but at roughly 0.5 au, the speed data plateaus while the model predicts an ongoing speed increase. In contrast, the model fits the magnetic field data remarkably well across all observed solar distances (0.06 to 79 au).

Plain Language Summary The solar wind is the hot, magnetized plasma that flows supersonically in all directions from the Sun into deep space. Its properties—including speed and magnetic field strength—are directly measured by spacecraft flying through it. A common means of studying the solar wind's expansion through the solar system is to examine how its properties vary on average with distance from the Sun. The Trans-Heliospheric Survey is a compilation of solar-wind data from 13 different spacecraft spanning over 60 years and ranging from the Sun's outer atmosphere to the outer solar system. These data were found to agree remarkably well with the Parker model of solar-wind expansion.

1. Introduction

In-situ observations of the solar wind across large temporal and spatial scales reveal clear "radial trends": the average changes in fluid parameters as a functions of radial distance, r, from the Sun. The notion of radial trends played a key role in the initial theory of the solar wind (Parker, 1958). Once the solar wind's supersonic flow was confirmed by observations from the Mariner 2 spacecraft (Neugebauer & Snyder, 1962), interplanetary missions became an important means by which theories of radial trends could be put to the test. Of particular note were the Helios 1 and 2 spacecraft, which provided in-situ observations of the solar wind from $r = 0.3$ to 1.0 au (from 1974 to 1985 and 1976–1989 respectively). Helios data revealed, for example, the solar wind's non-adiabatic expansion (Marsch, Schwenn, et al., 1982) and Coulomb collisional relaxation (Marsch, Rosenbauer, et al., 1982). Likewise, spacecraft such as Pioneer 10 and 11 (1972–1997 and 1973–1995) and Voyager 1 and 2 (1977 to present), which traveled to the solar system's outer planets, showed how the solar wind continues to evolve far from the Sun and demonstrated the effects of pickup ions on the plasma (Dyal, 1990; Kohlhase & Penzo, 1977; Stone, 1977). While the trajectories of most of the spacecraft remained close the Sun's equatorial plane, from 1999 to 2009 the Ulysses spacecraft's orbit carried it nearly over the Sun's poles, which enabled studies of how the solar wind varies with both radial distance and heliographic latitude (McComas et al., 2000).

The Trans-Heliospheric Survey compiles in-situ particle and field observations from these and other interplanetary spacecraft to better understand the solar wind's large-scale expansion and evolution. Version 1.0 (Maruca et al., 2023) incorporated data from 12 spacecraft: Parker Solar Probe (PSP), Helios 1 and 2, Mariner 2 and 10, Ulysses, Cassini, Pioneer 10 and 11, New Horizons, and Voyager 1 and 2. This present study utilized the latest version (Version 1.1) of the Trans-Heliospheric Survey, which includes additional data from PSP and New

Geophysical Research Letters 10.1029/2025GL115186

Horizons and (for the first time) data from Solar Orbiter. The Trans-Heliospheric Survey data spans over 60 years and over three orders of magnitude in distance from the Sun.

The analysis that accompanied Version 1.0 of the Trans-Heliospheric Survey (Maruca et al., 2023) focused on fitting radial trends in fluid parameters with broken power-laws. Though power laws (with and without breaks) have been used in many prior studies of radial trends (Bavassano et al., 2000, 2001; Hellinger et al., 2011; Maksimovic et al., 2005; Štverák et al., 2009, 2015), these models have little justification based on physical processes. In contrast, this study fits the bulk speed and magnetic field strength data from Version 1.1 of the Trans-Heliospheric Survey with the solar wind model introduced by Parker (1958). As detailed below, a strong agreement is found between the data and this model of the solar wind. Section 2 overviews the Parker (1958) solar-wind model, and Section 3 summarizes Version 1.1 of the Trans-Heliospheric Survey. The fitting of these data with the Parker (1958) model is detailed in Section 4, and conclusions appear in Section 5.

2. Background: The Parker Model

A prominent model for the solar wind's expansion through the heliosphere was developed by Parker (1958, 1965). This hydrodynamic model assumes a steady, spherically symmetric expansion of the solar wind from a source surface a few solar radii from the surface of the Sun. The equations governing this model are derived from the equation of motion for stationary expansion:

$$n_\mathrm{p} m_\mathrm{p} v_\mathrm{p} \frac{dv_\mathrm{p}}{dr} = -\frac{d}{dr}(2 n_\mathrm{p} k_\mathrm{B} T_\mathrm{p}) - G\frac{n_\mathrm{p} m_\mathrm{p} M_\odot}{r^2}, \tag{1}$$

where v_p, n_p, m_p, and T_p are respectively the proton bulk speed, number density, mass, and temperature. Likewise, k_B is the Boltzmann constant, G is the gravitational constant, and $M_\odot$ is the mass of the Sun. The left-hand side of Equation 1 represents the acceleration of the solar wind, and the right-hand side includes the terms for the forces acting on the solar wind: thermal pressure and gravity. Under the assumption of steady flow and conservation of particles, the solar wind is also governed by the continuity equation:

$$\frac{d}{dr}\left(n_\mathrm{p} v_\mathrm{p} r^2\right) = 0. \tag{2}$$

Parker (1958) introduced the dimensionless parameters:

$$\psi \equiv \frac{m_\mathrm{p} v_\mathrm{p}^2/2}{k_\mathrm{B} T_0}, \qquad \lambda \equiv \frac{G m_\mathrm{p} M_\odot}{2 a k_\mathrm{B} T_0}, \qquad \xi \equiv \frac{r}{a}, \qquad \text{and} \qquad \tau \equiv \frac{T_\mathrm{p}}{T_0}, \tag{3}$$

where a is the outer radius of the corona, and $T_0 \equiv T_\mathrm{p}(a)$ is the temperature of the outer corona. Combining Equations 1 and 2 eliminates n_p and, using these dimensionless parameters, gives

$$\frac{d\psi}{d\xi}\left(1 - \frac{\tau}{\psi}\right) = 2\xi^2 \frac{d}{d\xi}\left(\frac{\tau}{\xi^2}\right) - \frac{2\lambda}{\xi^2}. \tag{4}$$

Integrating this equation under the assumption that $T_\mathrm{p}(r)$ is constant for $r \geq a$ gives an implicit relation between ψ and ξ:

$$\psi - \ln\psi = -3 - 4\ln\frac{\lambda}{2} + \ln\xi + \frac{2\lambda}{\xi}. \tag{5}$$

This equation can be numerically solved for the explicit relation $\psi(\xi)$, which can then be converted into $v_\mathrm{p}(r)$ via Equation 3. The result is a trend in v_p that increases monotonically with r but at different rates depending on the choice of a and T_0.

Parker (1958) also introduced a model for the solar wind's magnetic field, **B**. Assuming that the solar wind's flow is completely radial in the reference frame rotating with the Sun, the field lines would trace out Archimedean spirals. The components of **B** in spherical coordinates are then (Burlaga, 1995),

$$
\begin{aligned}
B_r \quad (r,\theta,\phi) &= B_1\left(r_1,\theta,\phi-\frac{r\Omega}{v_{\mathrm{p}1}}\right)\left(\frac{r_1}{r}\right)^2 \\
B_\theta \quad (r,\theta,\phi) &= 0 \\
B_\phi \quad (r,\theta,\phi) &= B_1\left(r_1,\theta,\phi-\frac{r\Omega}{v_{\mathrm{p}1}}\right)\frac{r_1\Omega}{v_{\mathrm{p}1}}\left(\frac{r_1}{r}\right)\sin\theta.
\end{aligned}
\tag{6}
$$

Here, Ω is the Sun's equatorial rotation rate, and $B_1(r_1,\theta,\phi)$ is the radial component of the field at some arbitrary reference radius r_1. It is assumed that at r_1, the solar wind's acceleration can be neglected and that v_{p} remains constant at a value $v_{\mathrm{p}1}$. The term $\phi - r\Omega/v_{\mathrm{p}1}$ in B_1 accounts for the fact that as the solar wind propagates with speed v_{p1}, the region of the Sun that emitted the field rotates by an angle of $r_1\Omega/v_{\mathrm{p}1}$. In the ecliptic plane ($\theta = \pi/2$), the magnitude is,

$$
B = B_1\left(r_1,\theta,\phi-\frac{r\Omega}{v_{\mathrm{p}1}}\right)\sqrt{\left(\frac{r_1}{r}\right)^4+\frac{r_1^2\Omega^2}{v_{\mathrm{p}1}^2}\left(\frac{r_1}{r}\right)^2}.
\tag{7}
$$

For small r-values, the B_r term dominates B and causes it to scale approximately as r^{-2}. At large r-values, B_ϕ dominates B and gives it a r^{-1} dependency.

3. Data Analysis

Data in the Trans-Heliospheric Survey were taken from publicly available archives hosted on CDAWeb or OMNIWeb. This study used the newly prepared Version 1.1, which drew on all of the data used in Version 1.0 along with additional data from PSP and New Horizons and all-new data from Solar Orbiter. The process of combining the individual spacecraft data sets into a single data set for Version 1.1 was identical to that for producing Version 1.0, which is detailed by Maruca et al. (2023). A brief overview is provided here for the convenience of readers.

Figure 1 shows the radial coverage of the proton and/or magnetic field measurements from each of the 13 spacecraft used in Version 1.1. This information is also organized in Table 1 along with the maximum magnitude of heliographic latitude (λ) of each spacecraft. As was the case for Version 1.0 (Maruca et al., 2023), the Voyager 1 and 2 data sets were truncated at $r = 100$ au—well past the termination shock. Likewise, since both Versions 1.0 and 1.1 focused on in-plane observations, the Ulysses data after that spacecraft's Jovian encounter were excluded to avoid data from high latitudes.

Each spacecraft's data set was first averaged (as needed) to a uniform cadence of 1 hr. The results of the 1-hr averaging are shown for proton speed (v_{p}) in Figure 2 and for magnetic field strength ($B \equiv |\mathbf{B}|$) in Figure 3. In these figures, the distance from the Sun ranges from $r = 0.05$ to 100 au and has been divided into 85 logarithmically uniform bins. The upper plot in each of these two figures shows the number of one-hour intervals in each r-bin for the corresponding parameter (v_{p} or B). The middle plots of Figures 2 and 3 respectively show the median values of v_{p} and B for each spacecraft for each r-bin.

The top plots of Figures 2 and 3 are similar but not identical because, even on the same spacecraft, v_{p} and B are measured with distinct instruments. The difference is most pronounced with PSP observations, which show B-measurements extending closer to the Sun than the v_{p}-measurements. Following the example of Maruca et al. (2023), this study derived its PSP measurements from the `PSP_COHO1HR_MERGED_MAG_PLASMA` data set on CDAWeb. This data set took its thermal proton measurements from PSP's Faraday cup, which typically cannot provide proton moments during the mission's later perihelia, when the bulk of the solar wind is out of the instrument's field of view (see, e.g., Figure 9 by Kasper et al., 2016).

To address solar-cycle variations and other long-term fluctuations, Maruca et al. (2023) used "scaled" values based on the method introduced by C. W. Smith et al. (2001). To compute a scaled value of v_{p} or B (respectively denoted $\tilde{v}_{\mathrm{p}}$ and $\tilde{B}$), each 1-hr average value from a spacecraft was divided by a 27-day average-value near Earth ($r = 1$ au) from the OMNI data set. The particular 27-day average is specific to the time of the 1-hr spacecraft average and accounts for the transit time to/from $r = 1$ au. Thus,

10.1029/2025GL115186

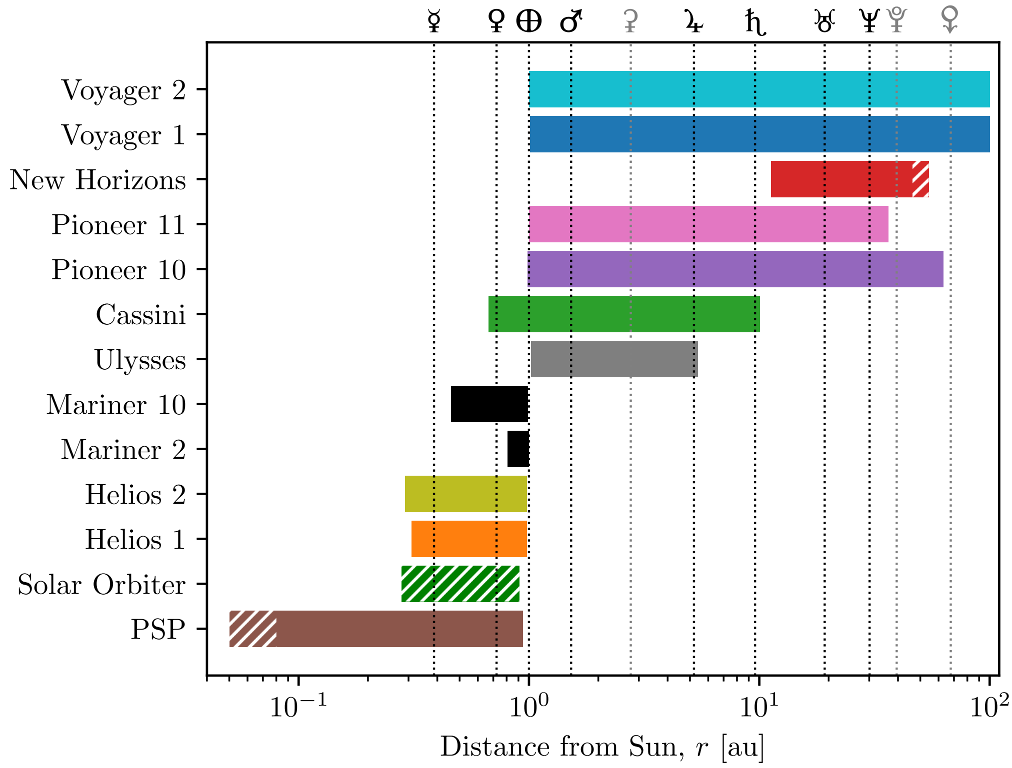

Figure 1. Radial coverage of each spacecraft included in Version 1.1 of the Trans-Heliospheric Survey. Vertical dotted lines display the semi-major axes of the orbits of the eight planets in black and three dwarf planets (Ceres, Pluto, and Eris) in gray. White hatches in the bars for Parker Solar Probe, Solar Orbiter, and New Horizons indicate data not present in Version 1.0.

$$\tilde{v}_{\mathrm{p}} = \frac{v_{\mathrm{p}}}{\langle v_{\mathrm{p}} \rangle_{\oplus}}, \text{ and } \tilde{B} = \frac{B}{\langle B \rangle_{\oplus}}, \tag{8}$$

where $\langle \cdots \rangle_{\oplus}$ denotes the 27-day average of OMNI data. The dots in the lower plots of Figures 2 and 3 respectively show the median values of $\tilde{v}_{\mathrm{p}}$ and $\tilde{B}$ across all spacecraft for each r-bin. The thick vertical lines indicate the 25th- and 75th-percentiles in each r-bin, and thin vertical lines indicate the 10th- and 90th-percentiles. The two right-most r-bins (shown in blue vs. magenta in these lower plots) contain spacecraft data influenced by the termination shock, and as a result have been excluded from the analysis detailed below.

In order to for any parameter (v_{p}, B, etc.) to be scaled, a valid measurement of the solar-wind speed is needed to correctly compute transit time to/from $r = 1$ au (see Equation 4 by Maruca et al., 2023). One consequence of this is that the data in the upper two plots of Figure 3 extend to lower r-values than the data in the bottom plot. As noted above, the v_{p}-values from PSP's Faraday cup do not extend as close to the Sun as the mission's B-measurements, so the B-measurements closest to the Sun cannot be scaled for lack of valid v_{p}-measurements.

Table 1
Table of Radial Distance, r, and Heliographic Latitude, λ, Coverage for Each Spacecraft

Spacecraft	r_{min} (au)	r_{max} (au)	max(|λ|)
PSP	0.05	1.0	4°
Solar Orbiter	0.3	1.0	8°
Helios 1	0.3	1.0	7°
Helios 2	0.3	1.0	7°
Mariner 2	0.8	1.0	8°
Mariner 10	0.6	1.0	7°
Ulysses	1.0	5.4	5°
Cassini	0.7	10.1	3°
Pioneer 10	1.0	63.0	8°
Pioneer 11	1.0	36.3	17°
New Horizons	11.3	54.4	5°
Voyager 1	1.0	100.0	34°
Voyager 2	1.0	100.0	27°

4. Results

The model introduced by Parker (1958) for solar-wind speed (Equation 5) indicates that v_{p} increases monotonically with r. Nevertheless, Figure 2 shows the (scaled) values of v_{p} increasing in the inner heliosphere before leveling off

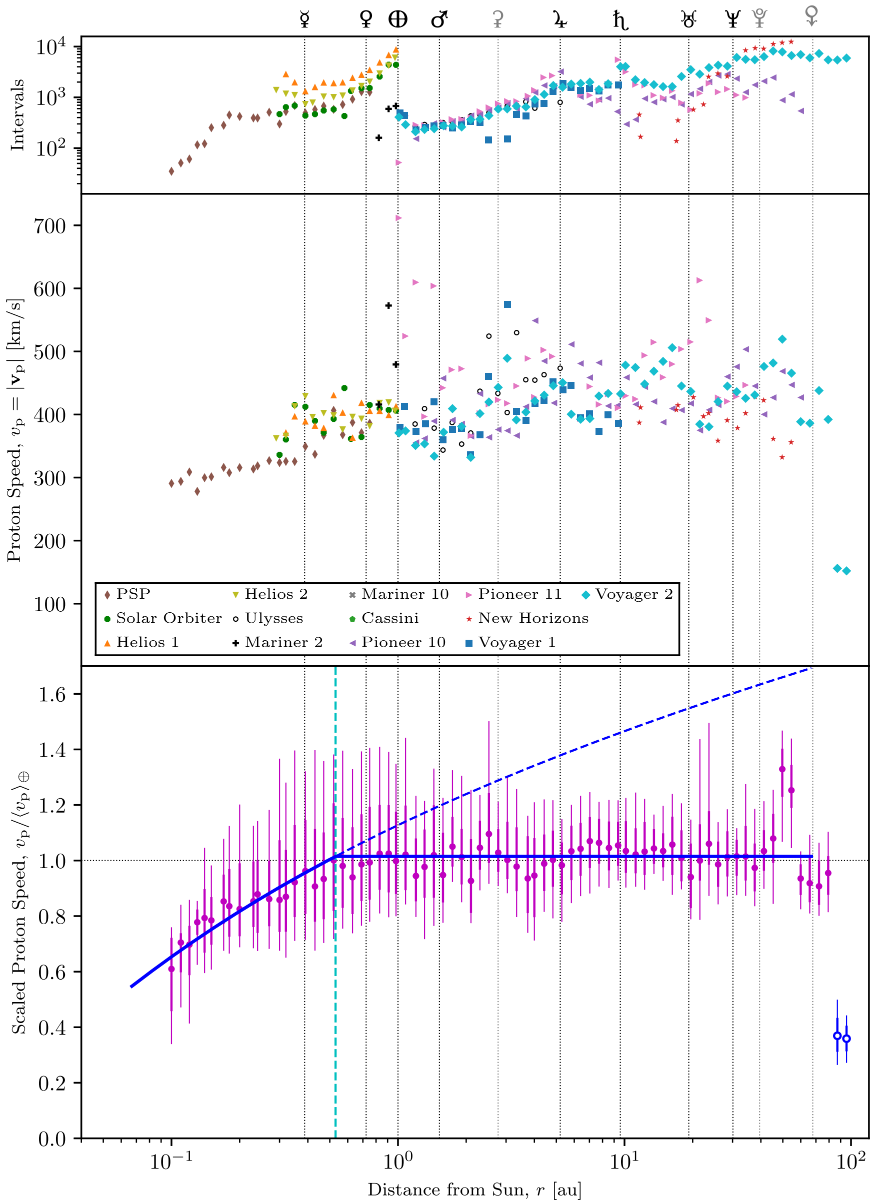

Figure 2. Analysis of proton bulk speed, v_p, versus radial distance, r. The top plot shows the number of one-hour intervals of v_p-data in each r-bin from each spacecraft. The middle plot shows the median v_p-value for each r-bin for each spacecraft. The bottom plot shows the scaled proton bulk speed, $\tilde{v}_p$ (Equation 8) across all spacecraft; circular markers indicate the median values, thick vertical bars indicating the 25th- and 75th-percentiles, and thin vertical bars indicating the 10th- and 90th-percentiles. The solid blue curve shows the fit of the piecewise Parker model (Equation 9), and the dashed blue line shows the continuation of the Parker model past the break point r_0 (vertical dashed cyan line). Vertical dotted lines across all plots indicate the semi-major axes of the orbits of the eight planets in black and three dwarf planets (Ceres, Pluto, and Eris) in gray.

at a steady value until the termination shock. To fit the radial trend in the median $\tilde{v}_p$-values, a piecewise model was chosen:

$$v_p(r) = \begin{cases} v_{\text{Parker}}(r) & r \le r_0 \\ v_{\text{Parker}}(r_0) & r_0 < r \end{cases}, \tag{9}$$

where $v_{\text{Parker}}(r)$ is from the solution of Equation 5.

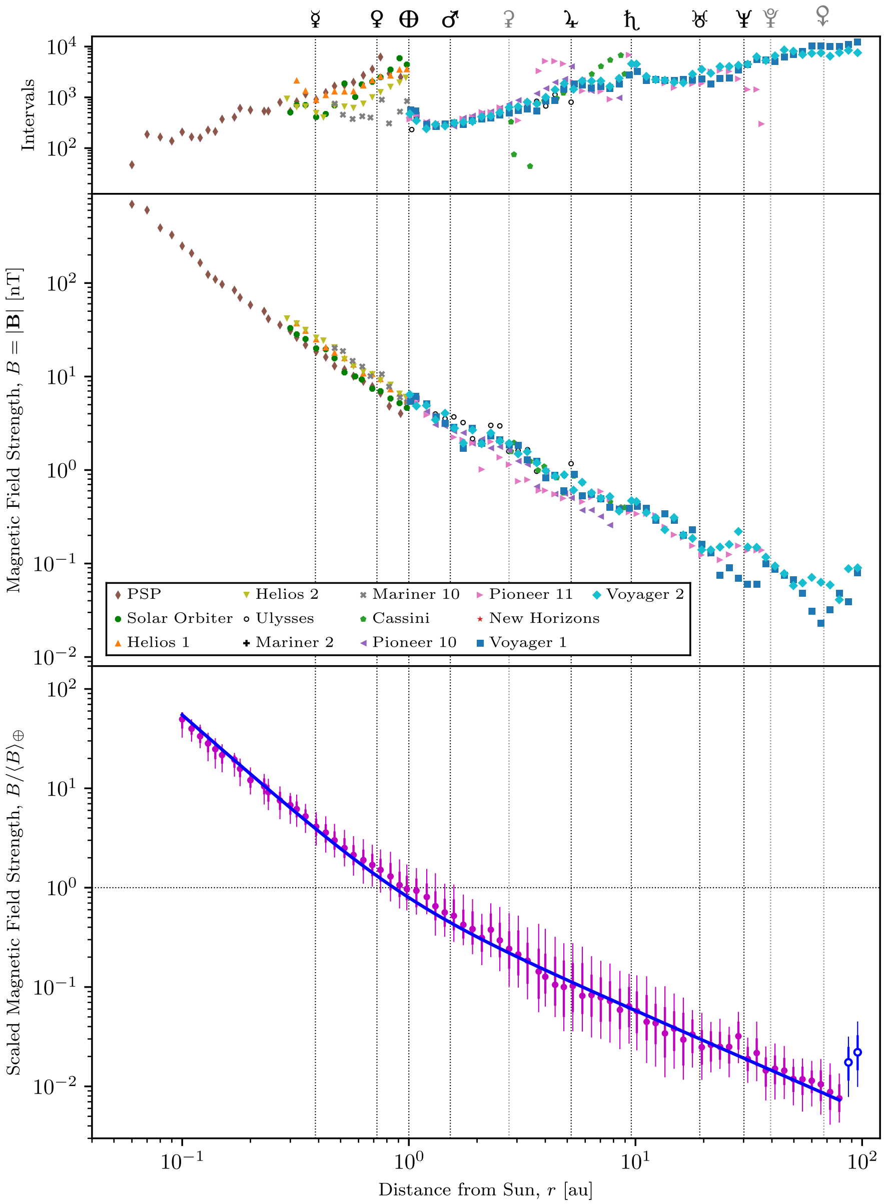

Figure 3. Analysis of magnetic field strength, $B \equiv |\mathbf{B}|$, versus radial distance, r. The top plot shows the number of 1-hr intervals of B-data in each r-bin from each spacecraft. The middle plot shows the median B-value for each r-bin for each spacecraft. The bottom plot shows the scaled magnetic field strength, $\tilde{B}$ (Equation 8) across all spacecraft; circular markers indicate the median values, thick vertical bars indicating the 25^{th}- and 75^{th}-percentiles, and thin vertical bars indicating the 10^{th}- and 90^{th}-percentiles. The solid blue curve shows the fit of the Parker model (Equation 7). Vertical dotted lines across all plots indicate the semi-major axes of the orbits of the eight planets in black and three dwarf planets (Ceres, Pluto, and Eris) in gray.

The solid blue curve in the lower plot of Figure 2 shows the best fit of Equation 9 to the median $\tilde{v}_{\mathrm{p}}$-values. Overall, this piecewise model shows very good agreement with the data. The model contained two free parameters. The first, the location of the break point, had a best-fit value of $r_0 = 0.530 \pm 0.052$ au. The second, the outer coronal temperature (implicit in the definition of ψ; see Equation 3) had a best-fit value of $9.36 \pm 0.22 \times 10^5$ K. Initially, third free parameter was considered: the outer radius of the corona, a (Equation 3). However, repeated fits consistently produced uncertainties in a that far exceeded its best-fit value, which suggested a weak sensitivity of the data to the value of a. Thus, following the example of Parker (1958), its value was fixed at $a = 10^9$ m.

Table 2
Table of Best-Fit Values From the Fits of $\tilde{v}_p$ and $\tilde{B}$

Parameter	Fit data	Best-fit value
T_0	$\tilde{v}_p$	$9.36 \pm 0.22 \times 10^5$ K
r_0	$\tilde{v}_p$	0.530 ± 0.052 au
$B_1 r_1^2$	$\tilde{B}$	3.001 ± 0.095 nT au^2
v_{p1}	$\tilde{B}$	413 ± 33 km/s

The Parker (1958) model for the magnitude of magnetic field (Equation 7) was used to fit the median $\tilde{B}$-values. Each value was assumed to have an uncertainty proportional to itself so that the fitting algorithm would give equal weight to data from the inner and outer heliosphere. The best-fit curve, shown in solid blue in the lower plot of Figure 3, shows excellent agreement with $\tilde{B}$-data across three orders-of-magnitude in r without any break points. This fit had two free parameters. First, the product $B_1 r_1^2$ was found to have a best-fit value of 3.001 ± 0.095 nT au^2. Second, the solar-wind speed had a best-fit value of $v_{p1} = 413 \pm 33$ km/s. The best-fit values from the fits of $\tilde{v}_p$ and $\tilde{B}$ are summarized in Table 2.

5. Conclusion

Figures 2 and 3 show a remarkable agreement between the latest version of the Trans-Heliospheric Survey data set and Parker's theoretical model of the solar wind (Parker, 1958).

The observed radial trend in proton speed, $v_p(r)$, aligns well with the Parker model in the inner heliosphere to a distance of $r_0 = 0.530 \pm 0.052$ au, at which point the speed plateaus out to the termination shock. An outer-heliospheric departure of $v_p(r)$ from the Parker model is expected, since a limitation of the model is that it predicts unbounded growth in speed. Despite this, interpreting the precise location of r_0 is complex. Recent observations show that both Alfvén wave energy deposition (Rivera et al., 2024) and thermal pressure gradients (Rivera et al., 2025) accelerate solar wind from different sources. The maximum speeds to which these mechanisms accelerate solar wind and the distances over which they operate are unknown. The Trans-Heliospheric Survey's coverage of solar activity is nonuniform, which impacts the solar wind sampled from the different source regions. Understanding the nonuniformity of the Trans-Heliospheric Survey's coverage, and its impact on r_0 is the subject of ongoing work. Nevertheless, the similarity in r_0 with the radial distance of Solar Orbiter during the radial conjunction of PSP and Solar Orbiter studied by Rivera et al. (2024) is striking.

Another limitation of the Parker (1958) model of the solar wind is its assumption of an isothermal temperature. In-situ solar wind observations show that T_p falls off appreciably (though not as quickly as would be expected from adiabatic expansion) with increasing r throughout the inner heliosphere (Marsch, Schwenn, et al., 1982; Maruca et al., 2023). Despite this inconsistency with T_p measurements, the Parker (1958) model still produces an excellent fit of the $v_p(r)$ close to the Sun and for $B(r)$ throughout the heliosphere. This suggests that the speed and magnetic field of the long-term-averaged steady-state solar wind behaves closely to the predictions of Parker (1958). Nevertheless, T_p measurements warrant a more exhaustive study that explores more complex models of the solar wind that better account for the observed trends in temperature. Some of these models may also be able to account for the plateau in $v_p(r)$ past r_0 observed in this study. In contrast, the Parker (1958) model predicts that $v_p(r)$ continue its monotonic increase throughout the heliosphere.

As Figure 2 shows, the solar wind experiences substantial, ongoing acceleration—well outside of the Alfvén region and almost to Earth's orbit—which complements the well established result of the solar wind's ongoing heating (Marsch, Schwenn, et al., 1982) and acceleration (Alterman, 2025; Rivera et al., 2024, 2025). Though many studies of solar-wind heating and acceleration often focus on processes occurring in the solar corona, these or other processes clearly extend beyond the corona and into the inner heliosphere. Further studies—including multi-point observations and simulations—are clearly warranted to improve understanding of the solar wind's evolution on its way to Earth and beyond. Quantifying the thermodynamic processes occurring in the inner heliosphere's "background" solar wind more accurately may serve to better simulations of the CME and space-weather events that propagate through this region.

In the region beyond r_0, the average speed data differ substantially from Equation 9. These values are due to circumstances and processes not included in the Trans-Heliospheric Survey's global model. First, the anomalously high speeds shown between $r \approx 45$–60 au, noted by Maruca et al. (2023), are due to the high-latitude position of Voyager 2 during solar minimum conditions (C. W. Smith et al., 2006). During this time, the average solar wind speed is latitudinally organized, with high-latitude speeds much faster than those at low latitude (McComas et al., 2008). When scaled with respect to the average speed in the low-latitude OMNI data at 1

Table 3
Table of Spacecraft Citations

Spacecraft	Citation
PSP	N. E. Papitashvili (2020)
Solar Orbiter	N. Papitashvili (2024)
Helios 1	Nes and Mariani (2021a)
Helios 2	Ness and Mariani (2021b)
Mariner 2	N. Papitashvili (2025a)
Mariner 10	N. Papitashvili (2025b)
Ulysses	Balogh and Mcomas (2021)
Cassini	Dougherty (2021)
Pioneer 10	E. J. Smith et al. (2023a)
Pioneer 11	E. J. Smith et al. (2023b)
New Horizons	Elliott et al. (2019)
Voyager 1	E. J. Smith et al. (2023b)
Voyager 2	Ness et al. (2023)
OMNI	King and Papitashvili (2020)

au, the speeds measured at Voyager 2 give consistently high values. This effect disappears on average during solar maximum, when the persistent latitudinal structure becomes disrupted. At that time, the Voyager 2 spacecraft has reached $r > 60$ au. Second, the reduced speeds shown beyond 60 au are due to the net deceleration of the solar wind from momentum loading by interstellar pickup hydrogen (Holzer, 1972; Isenberg, 1986; Isenberg et al., 2010). This is strictly an outer heliosphere effect, also not considered in the Trans-Heliospheric Survey's global model.

The radial trend in magnetic field strength, $B(r)$, agrees very closely with the Parker model across three orders of magnitude in r—from the closest available observations of PSP out to the termination shock. As noted above, one of the free parameters in the Parker model for $B(r)$ is the average solar-wind bulk speed, for which the data in Figure 3 have the best-fit value of 413 ± 33 km/s. For comparison, the 60-year median v_p-value in OMNI data was found to be 412 km/s (Maruca et al., 2023). The close agreement of these values is all the more remarkable given that they are derived from measurements made with entirely different instruments: magnetometers in of the fit parameter and particle instruments in the case of the OMNI average (Verscharen et al., 2019).

The consistency between the observed $v_p(r)$ and $B(r)$ trends and the Parker model is especially noteworthy given the simplicity of that model. Parker developed his model without the benefit of any in-situ observations of what he would only later dub the "solar wind." Partially for this reason, his model contained many assumptions that are now well known not to hold true. For example, the model assumes a steady, isotropic flow, though the solar wind has long been observed to consist of distinct and interacting streams of plasma with widely varying properties (see, e.g., Pizzo, 1978; Marsch, 1999; Marsch, 2006; Richardson, 2018, and references therein). Far from being steady, solar-wind plasma ubiquitously hosts strong fluctuations (e.g., waves and turbulence). The Trans-Heliospheric Survey data, though, have been heavily averaged (Maruca et al., 2023)—first to a one-hour cadence, and then across days or even years in the radial binning. With the original in-situ measurements spanning more than six decades, all of this averaging effectively smooths the vast majority of these fluctuations and transient phenomena. The results of this study indicate that what remains after this averaging—the "background" solar wind—is largely consistent with Parker's original predictions for speed and magnetic field strength.

Thus far, the Trans-Heliosheric Survey has focused on the solar wind's *overall* average behavior, but the radial trends likely exhibit significant variation both with solar-wind type (speed) and solar cycle. Both of these potential variations are currently being investigated and will be presented in forthcoming publications.

Data Availability Statement

The spacecraft data used for the Trans-Heliospheric Survey are from publicly available archives on CDAWeb and OMNIWeb Plus. For the specific dataset used for each spacecraft, see Table 1 of Maruca et al. (2023), who also provide the synthesized dataset for Version 1.0 of the Trans-Heliospheric Survey. Citations for the individual spacecraft datasets and OMNI data are organized in Table 3.

Acknowledgments
C.P.B., B.A.M., R.A.Q., B.L.A., and B.M.W. acknowledge support from NASA Grant 80NSSC22K0645. The work of B.A.M. on this research was supported by the International Space Science Institute in Bern, through ISSI International Team project 556 (Cross-Scale Energy Transfer in Space Plasmas; https://teams.issibern.ch/energtransferspaceplasmas/). P.A.I. is supported in part by NSF grant AGS2005982. B.L.A. acknowledges NASA grants 80NSSC22K0645 (LWS/TM) and 80NSSC22K1011 (LWS) along with Parker Solar Probe and Solar Orbiter funding at NASA Goddard. The authors extend their sincere thanks to both anonymous reviewers of this letter, whose many helpful suggestions significantly improved it.

References

Alterman, B. L. (2025). Characterizing the impact of Alfvén wave forcing in interplanetary space on the distribution of near-earth solar wind speeds. *The Astrophysical Journal Letters*, *984*(2), L64. https://doi.org/10.3847/2041-8213/add0a6

Balogh, A., & Mcomas, D. (2021). Ulysses merged magnetic field, plasma data. Retrieved from https://hpde.io/NASA/NumericalData/Ulysses/MAGandPLS/PT1H

Bavassano, B., Pietropaolo, E., & Bruno, R. (2000). On the evolution of outward and inward Alfvénic fluctuations in the polar wind. *Journal of Geophysical Research*, *105*(A7), 15959–15964. https://doi.org/10.1029/1999JA000276

Bavassano, B., Pietropaolo, E., & Bruno, R. (2001). Radial evolution of outward and inward Alfvénic fluctuations in the solar wind: A comparison between equatorial and polar observations by Ulysses. *Journal of Geophysical Research*, *106*(A6), 10659–10668. https://doi.org/10.1029/2000JA000453

Burlaga, L. F. (1995). *Interplanetary magnetohydrodynamics*. Oxford University PressNew. https://doi.org/10.1093/oso/9780195084726.001.0001

Dougherty, M. (2021). Cassini 1-min cruise phase magnetic field data in CDF format. Retrieved from https://hpde.io/NASA/NumericalData/Cassini/MAG/CDF/PT1M

Dyal, P. (1990). . *Pioneers 10 and 11 deep space missions (Technical Report No. NASA-TM-102269)*. NASA Ames Research Center. Retrieved from https://ntrs.nasa.gov/citations/19790003938

Elliott, H. A., McComas, D. J., Zirnstein, E. J., Randol, B. M., Delamere, P. A., Livadiotis, G., et al. (2019). Data from new horizons solar wind around Pluto (swap) instrument. Retrieved from https://cdaweb.gsfc.nasa.gov/misc/NotesN.html#NEW_HORIZONS_SWAP_SOLAR-WIND

Hellinger, P., Matteini, L., Štverák, Š., Trávníček, P. M., & Marsch, E. (2011). Heating and cooling of protons in the fast solar wind between 0.3 and 1 au: Helios revisited. *Journal of Geophysical Research (Space Physics)*, *116*(A9), 9105. https://doi.org/10.1029/2011JA016674

Holzer, T. E. (1972). Interaction of the solar wind with the neutral component of the interstellar gas. *Journal of Geophysical Research*, *77*(28), 5407–5431. https://doi.org/10.1029/JA077i028p05407

Isenberg, P. A. (1986). Interaction of the solar wind with interstellar neutral hydrogen: Three-fluid model. *Journal of Geophysical Research*, *91*(A9), 9965–9972. https://doi.org/10.1029/ja091ia09p09965

Isenberg, P. A., Smith, C. W., Matthaeus, W. H., & Richardson, J. D. (2010). Turbulent heating of the distant solar wind by interstellar pickup protons in a decelerating flow. *The Astrophysical Journal*, *719*(1), 716–721. https://doi.org/10.1088/0004-637x/719/1/716

Kasper, J. C., Abiad, R., Austin, G., Balat-Pichelin, M., Bale, S. D., Belcher, J. W., et al. (2016). Solar wind electrons alphas and protons (SWEAP) investigation: Design of the solar wind and coronal plasma instrument suite for solar probe plus. *Space Science Reviews*, *204*(1), 131–186. https://doi.org/10.1007/s11214-015-0206-3

King, J. H., & Papitashvili, N. E. (2020). *OMNI combined heliopheric observations (COHO), merged magnetic field, plasma and ephermeris, definitive hourly data*. NASA Space Physics Data Facility. Retrieved from https://hpde.io/NASA/NumericalData/OMNI/COHO/MergedMagPlasma/PT1H

Kohlhase, C., & Penzo, P. (1977). Voyager mission description. *Space Science Reviews*, *21*(2), 77–101. https://doi.org/10.1007/bf00200846

Maksimovic, M., Zouganelis, I., Chaufray, J.-Y., Issautier, K., Scime, E. E., Littleton, J. E., et al. (2005). Radial evolution of the electron distribution functions in the fast solar wind between 0.3 and 1.5 au. *Journal of Geophysical Research*, *110*(A9), A09104. https://doi.org/10.1029/2005JA011119

Marsch, E. (1999). Solar wind models from the sun to 1 AU: Constraints by in situ and remote sensing measurements. *Space Science Reviews*, *87*(1/2), 1–24. https://doi.org/10.1023/A:1005137311503

Marsch, E. (2006). Kinetic physics of the solar corona and solar wind. *Living Reviews in Solar Physics*, *3*, 1. https://doi.org/10.12942/lrsp-2006-1

Marsch, E., Rosenbauer, H., Schwenn, R., Mühlhäuser, K.-H., & Neubauer, F. M. (1982). Solar wind helium ions: Observations of the Helios solar probes between 0.3 and 1 au. *Journal of Geophysical Research*, *87*, 35–51. https://doi.org/10.1029/JA087iA01p00035

Marsch, E., Schwenn, R., Rosenbauer, H., Mühlhäuser, K.-H., Pilipp, W., & Neubauer, F. M. (1982). Solar wind protons: Three-dimensional velocity distributions and derived plasma parameters measured between 0.3 and 1 au. *Journal of Geophysical Research*, *87*, 52–72. https://doi.org/10.1029/JA087iA01p00052

Maruca, B. A., Qudsi, R. A., Alterman, B. L., Walsh, B. M., Korreck, K. E., Verscharen, D., et al. (2023). The trans-heliospheric Survey. *Radial trends in plasma parameters across the heliosphere*, *675*, A196. https://doi.org/10.1051/0004-6361/202345951

McComas, D. J., Barraclough, B. L., Funsten, H. O., Gosling, J. T., Santiago-Muñoz, E., Skoug, R. M., et al. (2000). Solar wind observations over Ulysses' first full polar orbit. *Journal of Geophysical Research (Space Physics)*, *105*(5), 10419–10433. https://doi.org/10.1029/1999JA000383

McComas, D. J., Ebert, R. W., Elliott, H. A., Goldstein, B. E., Gosling, J. T., Schwadron, N. A., & Skoug, R. M. (2008). Weaker solar wind from the polar coronal holes and the whole sun. *Geophysical Research Letters*, *35*(18), L18103. https://doi.org/10.1029/2008gl034896

Ness, N. F., & Mariani, F. (2021a). Helios 1 hourly merged magnetic field, plasma data. Retrieved from https://hpde.io/NASA/NumericalData/Helios1/MAGandPLS/PT1H

Ness, N. F., & Mariani, F. (2021b). Helios 2 hourly merged magnetic field, plasma data. Retrieved from https://hpde.io/NASA/NumericalData/Helios2/MAGandPLS/PT1H

Ness, N. F., Richardson, J. D., Burlaga, L. F., & Papitashvili, N. E. (2023). Voyager 2 hourly merged magnetic field and plasma data. *NASA Space Physics Data Facility*. https://doi.org/10.48322/VE5T-HF15

Neugebauer, M., & Snyder, C. W. (1962). Solar plasma experiment. *Science*, *138*(3545), 1095–1097. https://doi.org/10.1126/science.138.3545.1095.b

Papitashvili, N. (2024). Solar orbiter hourly merged magnetic field, plasma, and ephemeris, hourly data. Retrieved from https://hpde.io/NASA/NumericalData/SolarOrbiter/HelioWeb/Ephemeris/P1D

Papitashvili, N. (2025a). Mariner 2 merged magnetic field and plasma hourly data from Cohoweb service. Retrieved from https://omniweb.gsfc.nasa.gov/coho/form/mariner2.html

Papitashvili, N. (2025b). Mariner 10 merged magnetic field and plasma hourly data from Cohoweb service. Retrieved from https://omniweb.gsfc.nasa.gov/

Papitashvili, N. E. (2020). Parker solar probe (PSP) merged magnetic field, plasma, and ephemeris, hourly data. *NASA Space Physics Data Facility*. https://doi.org/10.48322/19ed-kz70

Parker, E. (1965). Dynamical theory of the solar wind. *Space Science Reviews*, *4*(5–6), 666. https://doi.org/10.1007/bf00216273

Parker, E. N. (1958). Dynamics of the interplanetary gas and magnetic fields. *The Astrophysical Journal*, *128*, 664. https://doi.org/10.1086/146579

Pizzo, V. (1978). A three-dimensional model of corotating streams in the solar wind, 1. theoretical foundations. *Journal of Geophysical Research*, *83*(A12), 5563–5572. https://doi.org/10.1029/ja083ia12p05563

Richardson, I. (2018). Solar wind stream interaction regions throughout the heliosphere. *Living Reviews in Solar Physics*, *15*(1), 1. https://doi.org/10.1007/s41116-017-0011-z

Rivera, Y. J., Badman, S., Verniero, J., Varesano, T., Stevens, M., Stawarz, J., et al. (2025). Differentiating the acceleration mechanisms in the slow and Alfvénic slow solar wind. *The Astrophysical Journal*, *980*(1), 70. https://doi.org/10.3847/1538-4357/ada699

Rivera, Y. J., Badman, S. T., Stevens, M. L., Verniero, J. L., Stawarz, J. E., Shi, C., et al. (2024). In situ observations of large-amplitude Alfvén waves heating and accelerating the solar wind. *Science*, *385*(6712), 962–966. https://doi.org/10.1126/science.adk6953

Smith, C. W., Isenberg, P. A., Matthaeus, W. H., & Richardson, J. D. (2006). Turbulent heating of the solar wind by newborn interstellar pickup protons. *The Astrophysical Journal*, *638*(1), 508–517. https://doi.org/10.1086/498671

Smith, C. W., Matthaeus, W., Zank, G., Ness, N., Oughton, S., & Richardson, J. (2001). Heating of the low-latitude solar wind by dissipation of turbulent magnetic fluctuations. *Journal of Geophysical Research*, *106*(A5), 8253–8272. https://doi.org/10.1029/2000ja000366

Smith, E. J., Gazis, P. R., & Papitashvili, N. E. (2023a). Pioneer 10 hourly merged magnetic field and plasma data. *NASA Space Physics Data Facility*. https://doi.org/10.48322/dn2j-fn46

Smith, E. J., Gazis, P. R., & Papitashvili, N. E. (2023b). Pioneer 11 hourly merged magnetic field and plasma data. *NASA Space Physics Data Facility*. https://doi.org/10.48322/VB0S-0W02

Stone, E. (1977). The voyager missions to the outer system. *Space Science Reviews*, *21*(2), 77–101. https://doi.org/10.1007/bf00200845

Štverák, Š., Maksimovic, M., Trávníček, P. M., Marsch, E., Fazakerley, A. N., & Scime, E. E. (2009). Radial evolution of nonthermal electron populations in the low-latitude solar wind: Helios, Cluster, and Ulysses observations. *Journal of Geophysical Research (Space Physics)*, *114*(A5), A05104. https://doi.org/10.1029/2008JA013883

Štverák, Š., Trávníček, P. M., & Hellinger, P. (2015). Electron energetics in the expanding solar wind via Helios observations. *Journal of Geophysical Research (Space Physics)*, *120*(10), 8177–8193. https://doi.org/10.1002/2015JA021368

Verscharen, D., Klein, K. G., & Maruca, B. A. (2019). The multi-scale nature of the solar wind. *Living Reviews in Solar Physics*, *16*(1), 5. https://doi.org/10.1007/s41116-019-0021-0